https://doi.org/10.5194/egusphere-2026-4057
Preprint. Discussion started: 20 August 2026

Optimized below-cloud scavenging scheme and its prominent performance of nitrogen wet deposition in polluted regions

Nuohang Liu[1,2], Baozhu Ge[1,*], Danhui Xu[3], Nan Yang[1,2], Xueshun Chen[1], Qixin Tan[4], Zifa Wang[1]

[1]State Key Laboratory of Atmospheric Environment and Extreme Meteorology, Institute of Atmospheric Physics, Chinese Academy of Sciences, Beijing, 100029, China
[2]University of Chinese Academy of Sciences, Beijing 100049, China
[3]National Center for Climate Change Strategy and International Cooperation, Ministry of Ecology and Environment, Beijing, 100035, China
[4]Chongqing Meteorological Observatory, Chongqing Meteorological Bureau, Chongqing, 401147, China

Correspondence author: Baozhu Ge (gebz@mail.iap.ac.cn)

Abstract. Simulations from Model Inter-Comparison Study for Asia (MICS-Asia) phase III generally underestimate regional nitrogen wet deposition, mainly because aerosol below-cloud scavenging processes are oversimplified or ignored in models. To address the problem, most existing studies adopt empirical corrections rather than optimizing physical mechanisms. This study develops an improved physically-based below-cloud wet scavenging parameterization scheme, which is implemented into the Nested Air Quality Prediction Model System (NAQPMS) for comparative simulations over East Asia in 2014. On the basis of conventional collision mechanisms, this scheme further incorporates three additional key mechanisms, including thermophoresis, diffusiophoresis and electrostatic interaction. The results show that the new scheme not only well captures the observed aerosols below-cloud scavenging coefficients, but also enables refined characterization of separate in-cloud and below-cloud wet deposition processes. Pronounced simulation improvements are found in heavily polluted regions including Beijing-Tianjin-Hebei region, Northeast China and Yangtze River Delta, while slight overestimation appears at several sites in Korea and Japan. Furthermore, the new scheme effectively elevates the contribution of below-cloud scavenging, especially for reduced nitrogen, achieving good agreement with observations in Beijing. Accurate simulations in both the in-cloud and below-cloud processes facilitate the reliable assessments of long-range transport and near-surface deposition fluxes of pollutants. This study demonstrates the necessity of fully resolving physically based wet scavenging mechanisms for high-precision nitrogen deposition modeling, which further advances our understanding of regional pollutant transport and the global nitrogen cycle.

1 Introduction

Wet scavenging is one of the major sinks of atmospheric nitrogen (Yu et al., 2019). The nitrogen wet deposition has attracted increasing attention worldwide due to its critical influence on many major contemporary environmental issues, such as air pollution (Luo et al., 2019), acidification (Du, 2018) and nutrient anomalies of ecosystems (Zhang et al., 2025; Zhang et al., 2022). Although the nitrogen deposition monitoring networks have been established in recent years, research into wet

https://doi.org/10.5194/egusphere-2026-4057
Preprint. Discussion started: 20 August 2026

deposition is still constrained by the spatial heterogeneity and limited temporal coverage of the observational data (Ge et al., 2020; Lue and Tian, 2007). Chemical transport models (CTMs) are usually used as an alternative operation to overcome the drawbacks, and are employed to investigate the long-term trends as well as the factors that affect nitrogen wet deposition over the world (Ge et al., 2020; Ponette-Gonzalez et al., 2022; Theobald et al., 2019; Vet et al., 2014). China is one of the three regions with the highest nitrogen deposition in the world (Yu et al., 2019). However, simulations of nitrogen wet deposition in China show varying degrees of underestimations (Ge et al., 2020; Tan et al., 2022). Moreover, the Model Inter-Comparison Study for Asia (MICS-Asia) phase III found that CTMs in East Asia also predicted lower values than measured in East Asia (Ge et al., 2020; Itahashi et al., 2020). The underestimation of nitrogen wet deposition is closely related to the uncertainty of discharge inventories and incomplete understanding of the chemical mechanisms. Moreover, inaccurate modeling of wet scavenging mechanisms also contributed to the underestimates produced by the current CTMs (Ge et al., 2020; Wang et al., 2008).

There are two main processes in wet deposition: in-cloud (rainout process) and below-cloud (washout process) scavenging (Seinfeld and Pandis, 2006; Tang et al., 2006). Previously, below-cloud wet scavenging was thought to be less important than in-cloud wet scavenging on a global or regional scale and was therefore simplified or even ignored in most CTMs (Bae et al., 2010; Environ.Inc, 2013; Roselle and Binkowski, 1999; Ryu and Min, 2022; Simpson et al., 2003; Tang et al., 2006). This simplification is valid in clean areas but inappropriate for heavily polluted regions. Based on field measurements, below-cloud wet deposition could account for at least 50 % of second inorganic aerosols sulfate, nitrate and ammonium wet deposition in heavy pollution regions, such as North China (Ge et al., 2016; Xu et al., 2017) and India (Chatterjee et al., 2010) based on field measurement data. Moreover, observation-based studies have demonstrated that extreme precipitation events can scavenge over 80 % of below-cloud ammonium and nitrate in heavily polluted regions (Pan et al., 2017), and even continuous light rain can remove at least 40 % of below-cloud ammonium and nitrate (Kulshrestha et al., 2009). Therefore, the underestimation of below-cloud scavenging and deposition by CTMs is a key factor contributing to the underestimation of nitrogen wet deposition in heavily polluted regions.

This study employs the Nested Air Quality Prediction Model System (NAQPMS) model to investigate the below-cloud wet scavenging of atmospheric nitrogen in East Asia, with a focus on China. Previous studies aimed at empirical formulas rather than physical mechanisms when improving below-cloud wet scavenging processes in CTMs (Fang et al., 2022; Ryu and Min, 2022; Wang et al., 2014a; Yao et al., 2024). In contrast, a theory-based below-cloud wet scavenging scheme is developed in this study to improve the simulation of the processes. The new scheme is implemented in the NAQPMS model and is evaluated against observational data, along with other classical wet deposition schemes in the model. This study also quantifies how the new scheme alters contributions from in-cloud and below-cloud scavenging, as well as the transport of nitrogen from source to downwind regions. The newly developed scheme proposed in this study can be implemented in other CTMs. Thus, it enables more accurate simulation of nitrogen wet deposition and deepens insights into the corresponding environmental impacts throughout China, East Asia, and global nitrogen deposition hotspots.

https://doi.org/10.5194/egusphere-2026-4057
Preprint. Discussion started: 20 August 2026

2 Data and methods

2.1 Model description and set up

NAQPMS is a three-dimensional Eulerian Chemical Transport Model, which was developed at the Institute of Atmospheric Physics, Chinese Academy of Sciences (Li et al., 2008; Li et al., 2011; Wang et al., 2006; Wang et al., 2026). This 3-D model includes chemical reactions, advection, diffusion, and dry and wet deposition processes, and a more detailed description of the model can be found in Li et al. (2012). Since this study focuses on updated wet deposition mechanisms, a detailed description of the corresponding scheme is presented in Sect. 2.2.

The domain used in this study covers most region of East Asia, with 182×172 grid cells at a horizontal resolution of 45 km. The model uses 20 terrain-following layers from the surface to 20 km altitude, with the lowest 9 layers below 2 km. The simulation period covers the year 2014, and the model runs for three month each time and a 5-day spin-up is performed in each run. The global chemistry transport model, Model for Ozone and Related Chemical Tracers (MOZART) version 2.4, provides initial and lateral boundary conditions for NAQPMS. The 2010 MIX Asian anthropogenic emission inventory developed for MICS-Asia III (Li et al., 2017) is adopted as the baseline dataset, followed by the adjustion from satellite-retrieved vertical column densities of AOD, SO_2, NO_x and NH_3 retrieved in 2014. Biogenic and biomass burning emissions are obtained from the Model of Emissions of Gases and Aerosols from Nature (MEGAN) v2.04 (Guenther et al., 2006) and the Global Fire Emission Database (GFED) (Van Der Werf et al., 2010), respectively.

The meteorological fields for the NAQPMS model are provided by the WRF model (the Weather Research and Forecasting model) version 4.0 (Skamarock et al., 2019), which is driven by the FNL reanalysis data. The physical parameterization schemes used for the WRF simulation are detailed in Table S1.

2.2 Methodology for wet deposition

2.2.1 Control experiment for wet deposition

The wet deposition schemes in the NAQPMS model similar with that in most CTMs is represent by:

$$\frac{dN}{dt} = -\Lambda N \,, \tag{1}$$

Where Λ is the wet scavenging coefficients of aerosols, N denotes the molar concentration of aerosols. During the development of the NAQPMS model, a wet deposition scheme similar to that of the Comprehensive Air Quality Model with Extensions (CAMx) model was originally adopted (Chen, 2013; Environ.Inc, 2013; Guo, 2013), which includes in-cloud and below-cloud wet scavenging processes. Both processes are described by the same formula (shown in the second row from bottom of Table S2), which is parameterized by collision efficiency, precipitation rate and raindrop diameter. For below-cloud scavenging processes, the collision efficiency between aerosols and raindrops is the sum of the efficiencies of the three conventional collision mechanisms: Brownian diffusion, directional interception and inertial impaction (formulas and descriptions are provided in Table S2 and Sect. S1). Regarding in-cloud scavenging, all aerosols within cloud layers are

https://doi.org/10.5194/egusphere-2026-4057
Preprint. Discussion started: 20 August 2026

assumed to exist within cloud water, and a collision efficiency is set to 0.9. For clarity and distinction, this wet deposition scheme is termed the "CAMx" scheme.

To more accurately simulate how in-cloud microphysics and chemistry affect in-cloud scavenging, Ge et al. (2014) adopted a new scavenging scheme analogous to the cloud process scheme in CMAQ v4.7, which includes both a grid-scale cloud scheme and a diagnostic convective cloud scheme. It is referred to as the "Ge14" scheme. However, this scheme assumes identical wet scavenging coefficients (formula shown in the first row from bottom of Table S2) for both in-cloud and below-cloud processes. Although it delivers a reasonable representation of in-cloud processes, the wet scavenging coefficient for in-cloud processes is far higher than that for below-cloud processes (typically by two orders of magnitude), which consequently lead to excessive removal of atmospheric pollutants (Itahashi et al., 2018; Shimadera et al., 2015). To address this issue, we first introduce the below-cloud wet scavenging process of the "CAMx" scheme into the "Ge14" scheme, producing an intermediate version termed the combined "Ge14-CAMx" scheme.

2.2.2 Update of below-cloud wet scavenging mechanism

Although below-cloud scavenging is explicitly represented in both the CAMx and Ge14-CAMx schemes, these models only consider three conventional collision mechanisms. This causes the below-cloud wet scavenging coefficients (BWSCs) with aerosol sizes of 0.1-2.5 μm to be underestimated by roughly 1-2 orders of magnitude (Bae et al., 2010; Xu et al., 2019a). Many studies have employed empirical formulas ($\Lambda=ap^b$) to improve the estimation of the BWSCs by CTMs (Fang et al., 2022; Ryu and Min, 2022; Wang et al., 2014a; Yao et al., 2024). Later versions of CAMx artificially increase fine-mode aerosol sizes by a factor of 10 to enhance BWSCs (Ramboll.Inc, 2024). However, these modifications lack physical basis. Furthermore, the absence of raindrop size distribution in the CAMx and Ge14-CAMx schemes can introduce biases into the characterization of BWSCs (Lu and Fung, 2018). Accordingly, a new wet scavenging scheme, referred to as the "Ge14-BWSC" scheme, is developed. The BWSCs of aerosols in this scheme are theoretically calculated as:

$$\Lambda = \int_0^\infty \frac{\pi}{4} {D_p}^2 U_t(D_p) E(D_p, d_p) N(D_p) dD_p \ , \quad (2)$$

Where D_p is the raindrop diameter, d_p is the aerosol diameter, $E(D_p, d_p)$ is the collision efficiency between raindrops and aerosols, $U_t(D_p)$ is the falling velocity of raindrops, $N(D_p)$ is the raindrop size distribution. In addition to the three conventional collision mechanisms, three new mechanisms, thermophoresis, diffusiophoresis and electrostatic interaction, are considered in $E(D_p, d_p)$. Their formulas and descriptions are provided in Table S2 and Sect. S1. As shown in Fig. S1, the efficiency of each collision mechanism can be calculated as a function of aerosol size. For d_p < 0.1 μm, Brownian diffusion is the dominant mechanism. For d_p > 2.5 μm, directional interception and inertial impaction become the primary mechanisms. For d_p between 0.1 and 2.5 μm, all the conventional mechanisms are weak, resulting in the lowest collision efficiency; hence, the size range is called the Greenfield gap. However, the three new mechanisms significantly enhance the collision efficiency within the Greenfield gap by an order of magnitude.

https://doi.org/10.5194/egusphere-2026-4057
Preprint. Discussion started: 20 August 2026

Local raindrop size distribution was also measured. A laser raindrop spectrograph (OTT Parsivel 2, Germany) was used for one-year field observation campaign (the measurement details are provided in Sect. S2) in Beijing. The measured raindrop spectra was processed to obtain the average observed raindrop size distribution for mixed cloud precipitation. In order to derive the convective cloud precipitation, raindrop spectra with reflectivity >38 dBZ and precipitation intensity >5 mm h^{-1} were selected. Previous studies have shown that the differences in types of raindrop size distribution have little effect on BWSCs compared with the collision mechanism (Mircea and Stefan, 1998; Wang et al., 2010). Here, an exponential distribution is used for fitting. Equation (3) is the averaged raindrop size distribution for mixed cloud precipitation during the observation period.

$$N(D_p) = 1.97 \times 10^{-2} exp(-4.8P^{-0.21}D_p)\,, \quad (3)$$

There is good correlation for the fitting equation of mixed cloud precipitation (R=0.97), but it is slightly worse for that of convective cloud precipitation (R=0.84) (Fig. S2a). Moreover, the number concentration of raindrops in convective cloud precipitation is greater than that in typical mixed cloud precipitation. As shown in Fig. S2b, for mixed cloud precipitation, the fitting equation fits well in the diameter range 0.06-2 mm, but slightly underestimates number concentration in larger diameters. The largest fitted raindrop particle diameter is around 2 mm, which is consistent with previous studies. Both traditional Marshall-Palmer (M-P) distribution and other logarithmic distributions have shown overestimation in small raindrops, indicating that they are not suitable in heavily polluted regions. Other studies have found that the gamma distribution (De Wolf, 2001) and the lognormal distribution (Cerro et al., 1997; Feingold and Levin, 1986) underestimate the overall number concentration of raindrops. Therefore, the fitted equation for typical mixed cloud precipitation is adopted in the Ge14-BWSC scheme to re-estimate BWSCs of aerosols.

Table 1 Summary of wet scavenging mechanisms of aerosols in the four schemes

Schemes	Below-cloud	In-cloud	Purpose
Ge14-BWSC	updated BWSC with new collision schemes and localized raindrop size distribution	cloud process scheme from CMAQ v4.7	This study
CAMx	conventional collision	collision efficiency set to 0.9	In cloud control experiment for Ge14-CAMx
Ge14	——	cloud process scheme from CMAQ v4.7	Below cloud control experiment for Ge14-CAMx
Ge14-CAMx	conventional collision	cloud process scheme from CMAQ v4.7	Below cloud control experiment for Ge14-BWSC

2.2.3 Other configurations for the wet deposition schemes

In this study, the four wet deposition schemes are integrated into the cloud module under a unified modeling framework. This consistent configuration ensures identical representations of subgrid convective transport and aqueous chemistry across the schemes, enabling a fair and quantitative intercomparison of their inherent differences in wet deposition simulation. For the CAMx, Ge14-CAMx and Ge14-BWSC schemes, the in-cloud and below-cloud wet scavenging processes in the grid scale cloud scheme are distinguished by cloud water content and rain water content, while in the diagnostic convective cloud

https://doi.org/10.5194/egusphere-2026-4057
Preprint. Discussion started: 20 August 2026

scheme, they are distinguished by cloud base height and precipitation rate. The summary of wet scavenging mechanisms of aerosols in these schemes is shown in Table 1. In addition, in the NAQPMS model, particulate NH_4^+ and NO_3^- are both assumed to reside in fine-mode size range (0.1-2.5 μm), and the geometric mean diameter is 0.5 μm (Xu et al., 2019a).

2.3 Observational Data

To evaluate the performance of the NAQPMS model in simulating nitrogen wet deposition, this study collected observation data in 2014 from the China National Environmental Monitoring Centre (CNEMC, http://www.cnemc.cn, last access: 6 June 2026) and the Acid Deposition Monitoring Network in East Asia (EANET, http://www.eanet.asia/, last access: 6 June 2026). The CNEMC dataset provides annual mean concentrations in precipitation and annual precipitation amounts for most regions in China. The EANET dataset provides monthly averaged concentrations in precipitation and monthly precipitation amounts for 13 countries in East Asia. Both datasets include concentrations in precipitation of nine inorganic ions: SO_4^{2-}, NO_3^-, NH_4^+, F^-, Cl^-, Ca^{2+}, Mg^{2+}, Na^+ and K^+. Furthermore, a quality control is applied to the observational data: for records with total ions concentrations in precipitation exceeding 100 $\mu eq \cdot L^{-1}$, the relative difference between total cation and total anion concentrations should be within 15 %-30 %; for those with total ion concentrations in precipitation between 50 and 100 $\mu eq \cdot L^{-1}$, the difference should be within 30 %-60 % (Rastogi and Sarin, 2005). After quality control, a total of 265 observation sites is retained, including 215 sites from CNEMC and 50 sites from EANET. The information of the sites is detailed in Table S3. Moreover, this study uses the atmospheric concentrations of major reactive nitrogen (N_r) species (including NH_3, NO_2, HNO_3, NH_4^+, NO_3^-) from Nationwide Nitrogen Deposition Monitoring Network (NNDMN) in 2014 (Xu et al., 2019b). The observational data have a monthly temporal resolution. After excluding sites with missing data, 27 sites are used for comparison. The information of these sites is shown in Table S4. However, this study does not use the observed wet deposition from NNDMN because precipitation samples are collected by open samplers and contain wet deposition and some dry deposition (i.e. bulk deposition) (Xu et al., 2018; Xu et al., 2015; Xu et al., 2019b).

For comparing model outputs with observational data, the simulated oxidized nitrogen (N_{ox}) wet deposition is the sum of wet deposition amounts of gaseous NO_x, HNO_3 and particulate NO_3^- output by the model, and the simulated reduced nitrogen (N_{rd}) wet deposition is the sum of the wet deposition amounts of gaseous NH_3 and particulate NH_4^+. The observed N_{ox} and N_{rd} wet deposition are corresponding to the wet deposition of NO_3^- and NH_4^+ at each observational site, respectively. The simulated total inorganic nitrogen (TIN) wet deposition is the sum of the simulated N_{ox} and N_{rd} wet deposition, while the observed TIN wet deposition is the sum of the observed NO_3^- and NH_4^+ wet deposition.

3 Results and discussion

3.1 Brief overview of the four schemes based on model validation

As precipitation is a key controlling factor for wet deposition estimates, we conduct intercomparison of annual precipitation amounts between model simulations and site observations to verify model performance prior to deposition analysis.

https://doi.org/10.5194/egusphere-2026-4057
Preprint. Discussion started: 20 August 2026

Comparisons between WRF-simulated precipitation and measurements from CNEMC and EANET (Fig. S3) shows the favorable agreement overall, with most simulated precipitation values falling within a factor of three of observations; nevertheless, the model presents systematic overprediction in annual precipitation, corresponding to an NMB of 29 %. Consistent with the positive precipitation bias from WRF simulations (Fig. S3), notable systematic overestimation is also identified in simulated N_{ox} wet deposition across the four parameterization schemes (Table 2). In contrast, simulated N_{rd} wet deposition is underestimated, which was also documented in prior MICS-Asia III modeling results (Ge et al., 2020; Itahashi et al., 2020). In terms of TIN wet deposition, the Ge14-BWSC scheme produces the smallest bias whereas Ge14 exhibits a positive bias and Ge14-CAMx together with CAMx feature substantial negative biases. Such bias patterns are further reproduced in annual mean concentrations in precipitation (Table 2), as all schemes overestimate N_{ox} yet underestimate those of N_{rd}. Owing to the positive precipitation bias in WRF outputs, the magnitude of biases in simulated TIN concentrations in precipitation depends on the sign of TIN wet deposition bias. Positive wet deposition offsets the precipitation overprediction and yields modest biases in TIN concentrations in precipitation, whereas negative wet deposition amplifies concentration biases. For the Ge14 scheme, this counterbalancing effect mitigates its positive bias in annual mean TIN concentrations in precipitation and brings the simulated concentrations closer to observations, with an NMB of 4 %. In contrast, the other three schemes exhibit amplified negative biases in TIN concentrations in precipitation because their wet deposition outputs are underestimated. Nevertheless, the Ge14 scheme still produces larger overall simulation errors relative to the Ge14-BWSC and Ge14-CAMx parameterizations. Its NME reaches 42 %, compared to 37 % for Ge14-BWSC and 36 % for Ge14-CAMx; the corresponding RMSE values are 1.3, 1.05 and 1.08, respectively. Furthermore, Ge14-BWSC best reproduces high annual rainwater TIN concentrations and performs well in heavily polluted regions (Fig. S4).

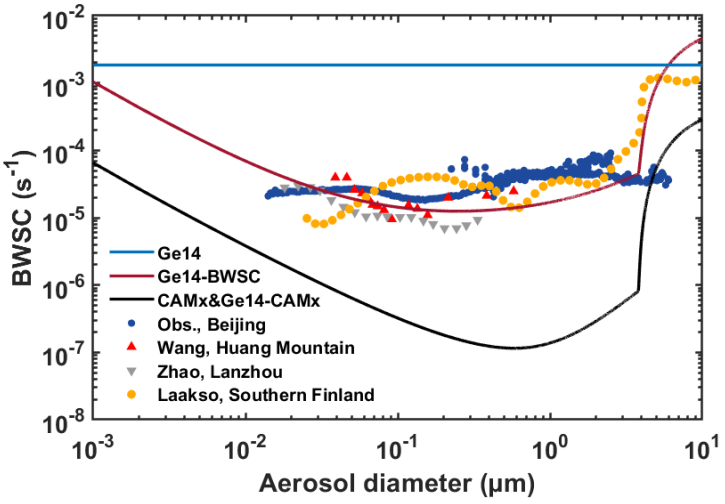

Figure 1. BWSCs calculated by the four schemes (rainfall rate: 1 mm h^{-1}) and comparison with those observed in Beijing and in other monitoring sites recorded by previous studies. They are plotted as a function of aerosol diameter.

https://doi.org/10.5194/egusphere-2026-4057
Preprint. Discussion started: 20 August 2026

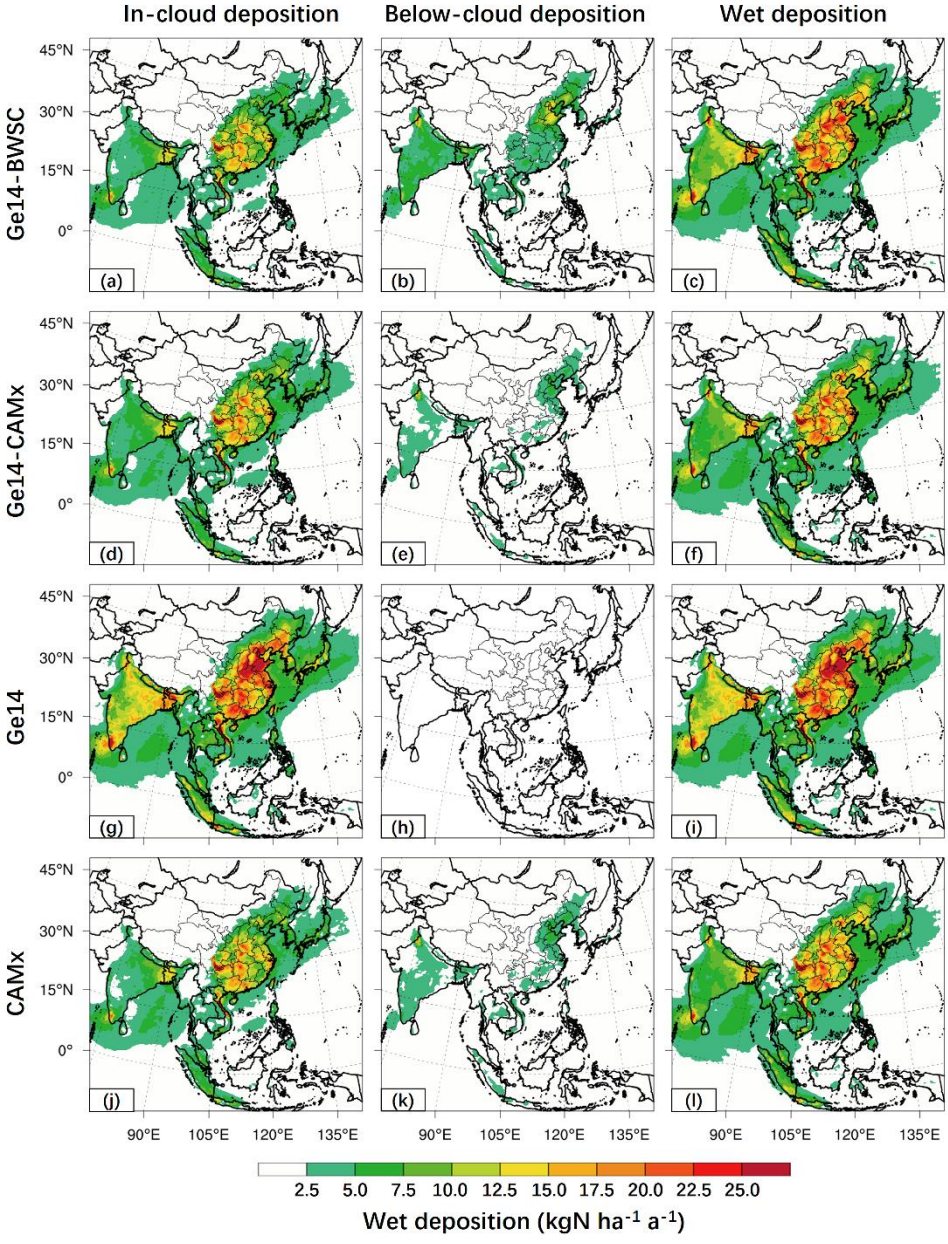

Figure 2. The spatial patterns of in-cloud, below-cloud and wet deposition of the Ge14-BWSC, Ge14-CAMx, Ge14 and CAMx schemes.

Figure 1 compares two groups of BWSCs: from the observational values including field measurements obtained at the Beijing site (see Sect. S3 for measurement details), and literature-reported data from other monitoring sites (Laakso et al., 2003; Wang et al., 2014b; Zhao et al., 2015), and simulated results by the four wet deposition schemes at a rainfall intensity of 1 mm h^{-1}. For the aerosol size range from 0.1 to 2.5 μm, the simulated BWSCs of Ge14-BWSC scheme show the best

https://doi.org/10.5194/egusphere-2026-4057
Preprint. Discussion started: 20 August 2026

agreement with the observations among all schemes. The BWSCs of the Ge14-CAMx and CAMx schemes are nearly two orders of magnitude lower than the observations. In contrast, those of the Ge14 scheme are 1-2 orders of magnitude higher than the observations, because it employes in-cloud scavenging coefficients to represent below-cloud scavenging processes (Ge et al., 2014; Lu and Fung, 2018; Roselle and Binkowski, 1999). The in-cloud, below-cloud and wet deposition of TIN simulated by the four schemes are shown in Fig. 2. Simulations from the four schemes reveal that the TIN wet deposition over Eastern China is markedly higher than that in other regions. The Ge14 scheme yields the highest annual wet deposition, followed by the Ge14-BWSC, Ge14-CAMx and CAMx schemes. This ranking agrees reasonably well with simulated BWSCs shown in Fig. 1. Specifically, the Ge14-BWSC scheme delivers the greatest below-cloud wet deposition and significantly exceeds the Ge14-CAMx and CAMx schemes, whereas the Ge14 scheme treats both in-cloud and below-cloud scavenging as in-cloud process, resulting in the largest deposition. Validation metrics confirm that Ge14-BWSC and Ge14-CAMx outperform the other two schemes, which indicate that accurate wet scavenging simulations need to physically separate in-cloud and below-cloud removal pathways and reasonably represent in-cloud convection. Between the two improved schemes, Ge14-BWSC is better than that of the Ge14-CAMx, suggesting the importance of the physically comprehensive and rational parameterization of below-cloud scavenging.

Table 2. Validation results of annual wet deposition and annual mean concentrations in precipitation of the four wet deposition schemes

Metrics			MM	MO	R	NMB	NME	RMSE
Annual wet deposition ($kgN\ ha^{-1}\ a^{-1}$)	CAMx	N_{ox}	7.04	5.57	0.45	27 %	62 %	4.46
		N_{rd}	5.05	8.96	0.48	-44 %	55 %	7.68
		TIN	12.09	14.53	0.52	-17 %	44 %	9.56
	Ge14	N_{ox}	8.61	5.57	0.39	55 %	80 %	5.59
		N_{rd}	7.16	8.96	0.37	-20 %	53 %	7.18
		TIN	15.77	14.53	0.43	9 %	51 %	10.13
	Ge14-CAMx	N_{ox}	7.24	5.57	0.44	30 %	64 %	4.57
		N_{rd}	5.25	8.96	0.47	-41 %	55 %	7.60
		TIN	12.49	14.53	0.51	-14 %	45 %	9.53
	Ge14-BWSC	N_{ox}	7.55	5.57	0.42	36 %	67 %	4.79
		N_{rd}	5.97	8.96	0.42	-33 %	53 %	7.36
		TIN	13.53	14.53	0.48	-7 %	46 %	9.59
Annual mean concentrations in precipitation ($mgN\ L^{-1}$)	CAMx	N_{ox}	0.81	0.76	0.61	7 %	50 %	0.58
		N_{rd}	0.59	1.19	0.73	-50 %	55 %	0.88
		TIN	1.4	1.95	0.76	-28 %	39 %	1.09
	Ge14	N_{ox}	1.08	0.76	0.59	42 %	71 %	0.86
		N_{rd}	0.96	1.19	0.75	-19 %	43 %	0.72
		TIN	2.03	1.95	0.75	4 %	42 %	1.30
	Ge14-CAMx	N_{ox}	0.85	0.76	0.61	12 %	52 %	0.60
		N_{rd}	0.63	1.19	0.74	-47 %	53 %	0.84
		TIN	1.48	1.95	0.76	-24 %	37 %	1.05
	Ge14-BWSC	N_{ox}	0.91	0.76	0.6	20 %	57 %	0.68
		N_{rd}	0.75	1.19	0.74	-37 %	47 %	0.75
		TIN	1.66	1.95	0.75	-15 %	36 %	1.08

Notes: MM is the mean value of model, MO is the mean value of observation, R is the correlation coefficient, NMB is the normalized mean bias, NME is the normalized mean error, RMSE is the root mean square error.

https://doi.org/10.5194/egusphere-2026-4057
Preprint. Discussion started: 20 August 2026

3.2 Comparison of atmospheric N_r and TIN concentration in precipitation across different regions

In order to evaluate the performance of the four wet deposition schemes in different regions, this study divides the land area within the domain into Region I, II and III (Fig. 3e). Region III covers areas outside China, while the territory within China is split into Region I and Region II. Region I includes the Beijing-Tianjin-Hebei (BTH) region, Northeast China and the Yangtze River Delta (YRD) region, while Region II covers South China, Southwest China, Northwest China and the Qinghai-Tibet Plateau. Region I is characterized as the most nitrogen-polluted area among the three regions, with both observational data and model simulations capturing its maximum annual mean TIN concentrations in precipitation (Fig. 3f). Regions II and III only emit less than one-third of Region I's total annual NO_x and NH_3 flux (Fig. S5), leading to their much lower TIN concentrations in precipitation. Consistently, observed atmospheric total N_r concentrations are higher in Region I than Region II (Fig. S6a and S6b). It is found that the Ge14-BWSC scheme has the best performance in Region I, with the lowest bias and the largest number of sites with normalized biases within ±15 % (Fig. 3a-d). The Ge14 scheme significantly overestimates the annual mean TIN concentrations in precipitation, while the Ge14-CAMx and CAMx schemes underestimate them. Further comparison of cumulative probability versus TIN concentrations in precipitation curves also reveal that Ge14-BWSC achieves better agreement with observations at high-TIN monitoring sites (Obs. > 3.0 mgN L^{-1}) (Fig. 4). The validation metrics of the Ge14-BWSC scheme, including NMB, NME, and RMSE, are better than those of the other schemes (Table S5).

Nevertheless, all schemes systematically underestimate the annual mean TIN concentrations in precipitation across Region II. Among them, the Ge14 scheme with the strongest wet scavenging effect yields the mildest underestimation and the largest number of sites whose normalized biases fall within ±15 %. This discrepancy is primarily driven by underestimated NH_3 emissions. The annual NH_3 emission over Region II adopted in our simulation is 4.3 Tg a^{-1}, while the MIXv2 emission inventory records a value close to 5.0 Tg a^{-1} (Li et al., 2024). Another reason is that precipitation in Region II is overestimated during summer (Fig. S6b), and the model may also simulate higher convective precipitation (especially in Southern China), accompanied by more frequent convective vertical transport, which carries excess N_r to downwind regions or above cloud tops, thereby reducing local surface concentrations of N_r and the fraction of N_r removed by wet scavenging. However, a further investigation of the impacts of convective transport is needed. Notably, the Ge14 scheme overestimates annual mean TIN concentrations in precipitation in Region I yet underestimates those in Region II. Therefore, its low overall bias listed in Table 2 does not reflect superior model performance but originates from mutually offsetting positive and negative biases between the two regions. In Region III, although the differences among the schemes are relatively small, the annual mean TIN concentrations in precipitation in Northeast Asia including Korea and Japan are overestimated, while those in Southeast Asia are generally underestimated by these schemes (Fig. 3a-d).

https://doi.org/10.5194/egusphere-2026-4057
Preprint. Discussion started: 20 August 2026

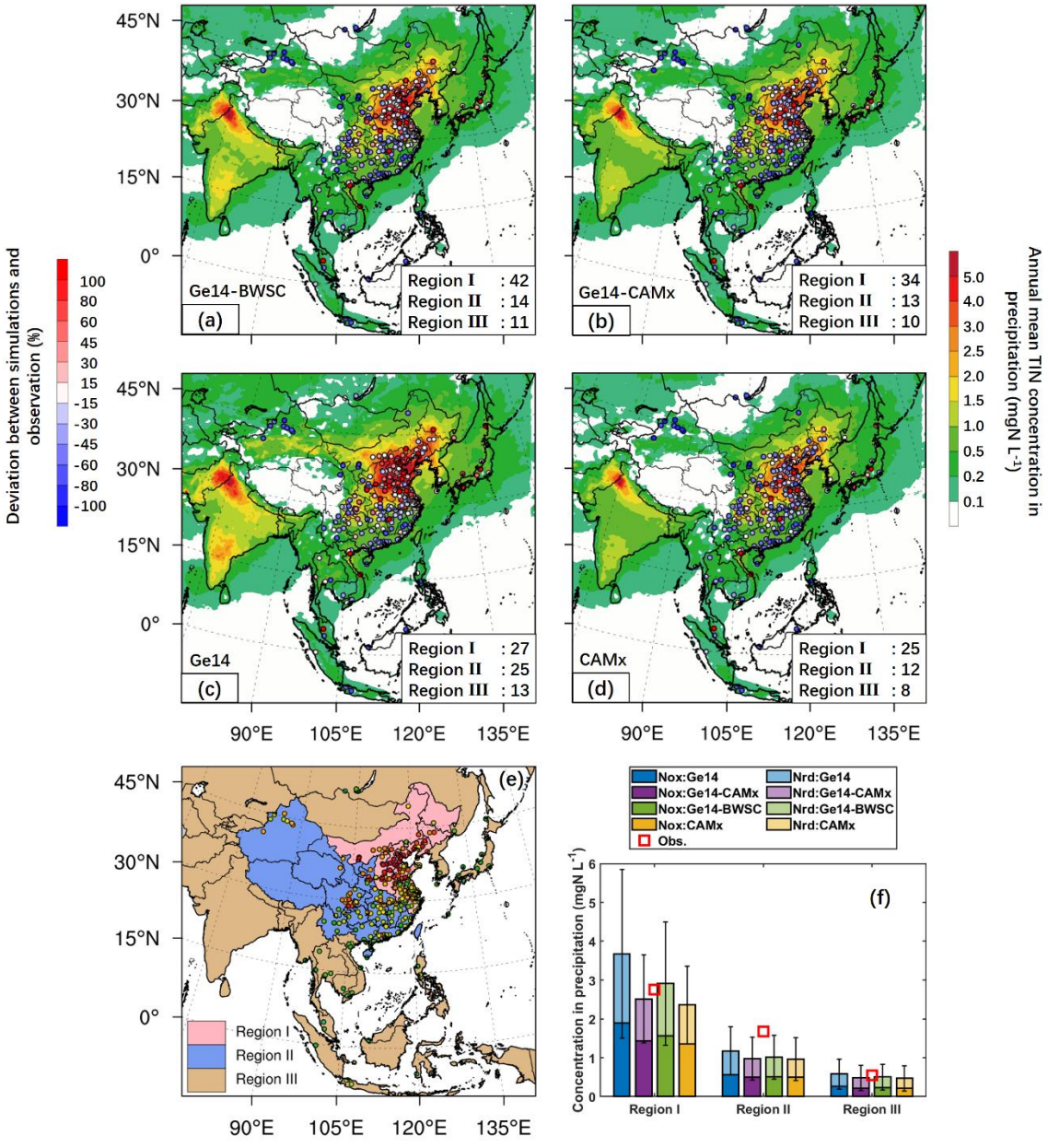

Figure 3. (a-d) The distributions of simulated annual mean TIN concentrations in precipitation by the four wet deposition schemes and normalized biases (defined as the difference between the simulated and observed value at a given site divided by the observed value) at each site marked by blue, white or red dots. The lower left box is the number of sites with normalized biases within ±15 % in Region I, II and III. (e) The observed annual mean TIN concentrations in precipitation and division of Region I, II and III. (f) The comparison of simulations and observations in Region I, II and III.

Figure S6 compares simulated and observed atmospheric concentrations of major N_r species to interpret the bias mechanisms in Region I and Region II. All schemes generally reproduce N_{ox} concentrations and seasonal variations in N_{rd} concentrations for both regions (Fig. S6a, S6c and S6e). However, N_{rd} concentrations and their proportions are

https://doi.org/10.5194/egusphere-2026-4057
Preprint. Discussion started: 20 August 2026

underestimated in all seasons, leading to the overestimation of contribution of N_{ox} to total N_r (Fig. S6b, S6d and S6f). The underestimation of N_{rd} can be attributed to lower annual NH_3 emissions in the model input compared with values reported in previous studies (Fig. S7). Meanwhile, simulated atmospheric concentrations of HNO_3 and NO_3^- are overestimated in both regions during summer, and further leads to overestimated N_{ox} wet deposition fluxes. Atmospheric NH_3 and NH_4^+ concentrations are underestimated year-round in Region II, which serves as the primary driver for the underestimated total N_r concentrations in this region. In contrast, Region I exhibits much milder underestimation of NH_3 and NH_4^+, resulting in closer agreement of simulated total N_r concentrations against measurements.

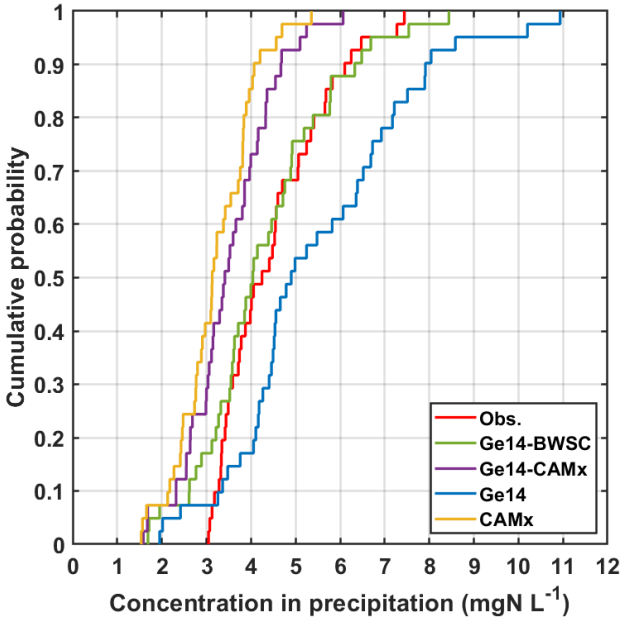

Figure 4. The comparison of cumulative probability versus TIN concentration in precipitation at high-TIN monitoring sites in Region I with the observed annual mean TIN concentrations in precipitation > 3.0 mgN L^{-1} (N=41).

3.3 Below-cloud contribution of N_{rd} and N_{ox}

Among the Ge14-BWSC, Ge14-CAMx and CAMx schemes, the regions with high below-cloud TIN contributions are mainly found in Northeast China, the BTH region, the Taklamakan Desert, the Gobi Desert, India and Indochina Peninsula (Fig. 5g-i). For Northeast China and the BTH region, below-cloud TIN contributions stand at roughly 30 %–40 % under the Ge14-CAMx scheme and 40 %–50 % under the default CAMx scheme. Both of these two schemes underestimate annual mean TIN concentrations in precipitation. The Ge14-BWSC framework incorporates revised aerosol below-cloud wet scavenging mechanisms. This adjustment lifts regional below-cloud TIN contributions to 60 %–70 % within the above areas. The Ge14-BWSC scheme therefore delivers the closest consistency with field observations.

Figure 6 presents the comparisons of below-cloud contributions of N_{ox} and N_{rd} simulated by the Ge14-BWSC and Ge14-CAMx schemes against Beijing observational data from summer and autumn of 2014 (Ge et al., 2021; Xu et al., 2017). The CAMx scheme is excluded from the comparison because it performs most poorly among the three schemes in simulating the

https://doi.org/10.5194/egusphere-2026-4057
Preprint. Discussion started: 20 August 2026

annual mean TIN concentration in precipitation. The arithmetic means of the below-cloud contributions of N_{ox} for the Ge14-BWSC and Ge14-CAMx schemes are 65.6 % and 51.7 %, respectively, and those for N_{rd} are 67.2 % and 28.5 %, respectively. Compared with the Ge14-CAMx scheme, the Ge14-BWSC scheme shows better agreement with the observations (65.3 % for N_{ox} and 68.2 % for N_{rd}). Furthermore, Ge et al. (2016) reported that the below-cloud contributions of N_{ox} and N_{rd} at Dandong and Dalian in Northeast China were 50 %-92 % and 46 %-85 %, respectively. The Ge14-CAMx scheme estimates that the below-cloud contributions are approximately 30 %-50 % for N_{ox} and 10 %-20 % for N_{rd}, while the Ge14-BWSC scheme estimates that the below-cloud contributions are 40 %-60 % for both N_{ox} and N_{rd}, which is closer to the observations. Hence, the updated below-cloud wet scavenging mechanisms for aerosols effectively improves the model's underestimation of below-cloud contributions in heavily polluted regions, especially for N_{rd}.

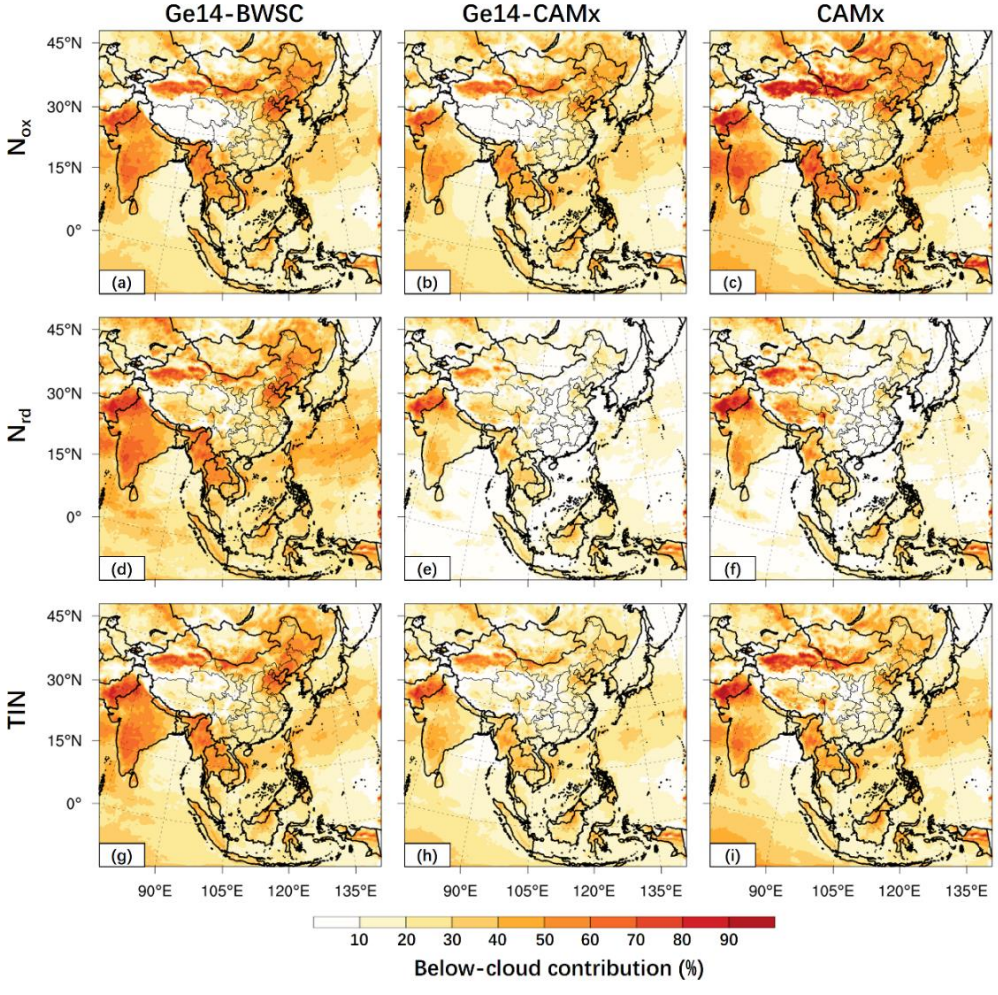

Figure 5. The spatial patterns of the annual below-cloud contribution of N_{ox}, N_{rd} and TIN in the Ge14-BWSC, Ge14-CAMx and CAMx schemes.

https://doi.org/10.5194/egusphere-2026-4057
Preprint. Discussion started: 20 August 2026

In the Ge14-CAMx and CAMx schemes, the below-cloud contribution of N_{rd} is lower than that of N_{ox}, whereas N_{ox} and N_{rd} below-cloud contributions are similar in the Ge14-BWSC scheme (Fig. 5a-e). This is because the below-cloud deposition in the Ge14-CAMx and CAMx schemes relies almost solely on gaseous substances dominated by HNO_3 for N_{ox} and NH_3 for N_{rd} without reflection of aerosol below-cloud scavenging (Fig. S8b). This explains why the updated CAMx model artificially enlarges fine-mode aerosol sizes by a factor of 10 to strengthen below-cloud scavenging processes (Ramboll.Inc, 2024). HNO_3 has a higher Henry's law coefficient than NH_3, the below-cloud deposition of HNO_3 is 3-4 times that of NH_3, making the below-cloud deposition of N_{ox} more than three times higher than that of N_{rd} in the Ge14-CAMx and CAMx schemes. By contrast, in-cloud deposition is dominated by aerosols, and the in-cloud depositions of particulate NH_4^+ and particulate NO_3^- are comparable (Fig. S8a). Although the in-cloud deposition of HNO_3 is still higher than that of NH_3, but this only makes the in-cloud deposition of N_{ox} higher than that of N_{rd} by about 25 %-30 % (Fig. S8a). Therefore, HNO_3 contributes more to the below-cloud contribution of N_{ox} than NH_3 contributes to that of N_{rd}, resulting in a higher below-cloud contribution for N_{ox} than for N_{rd}. However, the Ge14-BWSC scheme increases the effects of below-cloud scavenging of aerosols, especially particulate NH_4^+, thereby narrowing the difference between the below-cloud contributions of N_{ox} and N_{rd}. Compared with the Ge14-CAMx scheme, the Ge14-BWSC scheme shows a greater increase in the below-cloud contribution for N_{rd} than for N_{ox} (Fig. 5a-b and 5d-e). This discrepancy arises primarily from the higher atmospheric mass concentration of particulate NH_4^+ relative to NO_3^- as illustrated in Fig. S6e. Ambient particulate NH_4^+ preferentially forms low-volatile $(NH_4)_2SO_4$ before generating semi-volatile NH_4NO_3. Low-volatile $(NH_4)_2SO_4$ is efficiently washed out by rainfall and raises the below-cloud deposition flux of N_{rd}. Semi-volatile NH_4NO_3 can undergo re-volatilization back to the atmosphere, which further limits the increase in below-cloud deposition of N_{ox}.

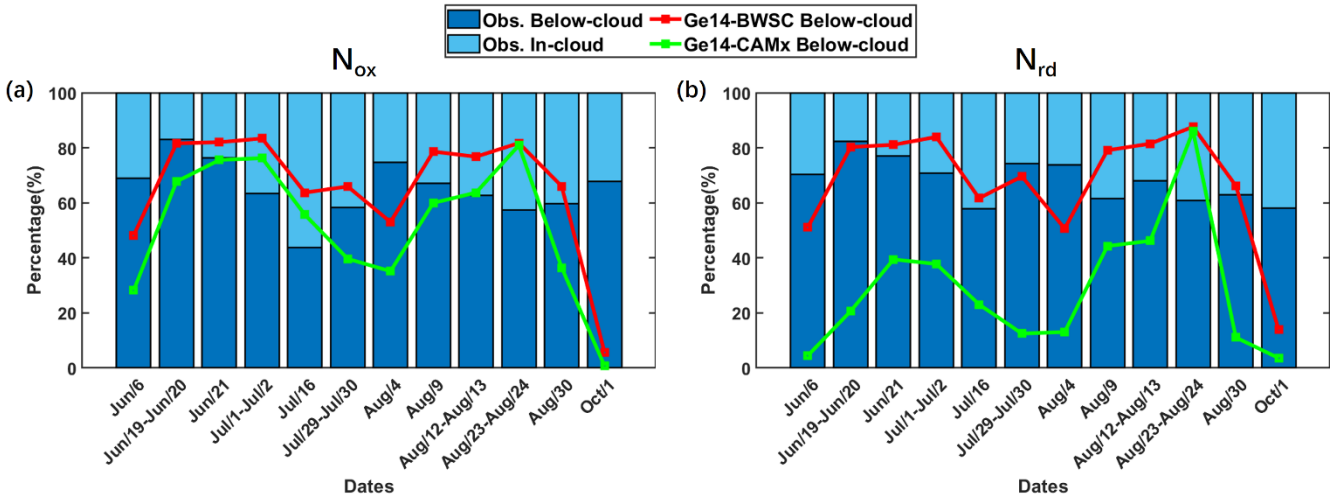

Figure 6. The observed and simulated below-cloud contributions of (a) N_{ox} and (b) N_{rd} by the Ge14-BWSC and Ge14-CAMx schemes.

https://doi.org/10.5194/egusphere-2026-4057
Preprint. Discussion started: 20 August 2026

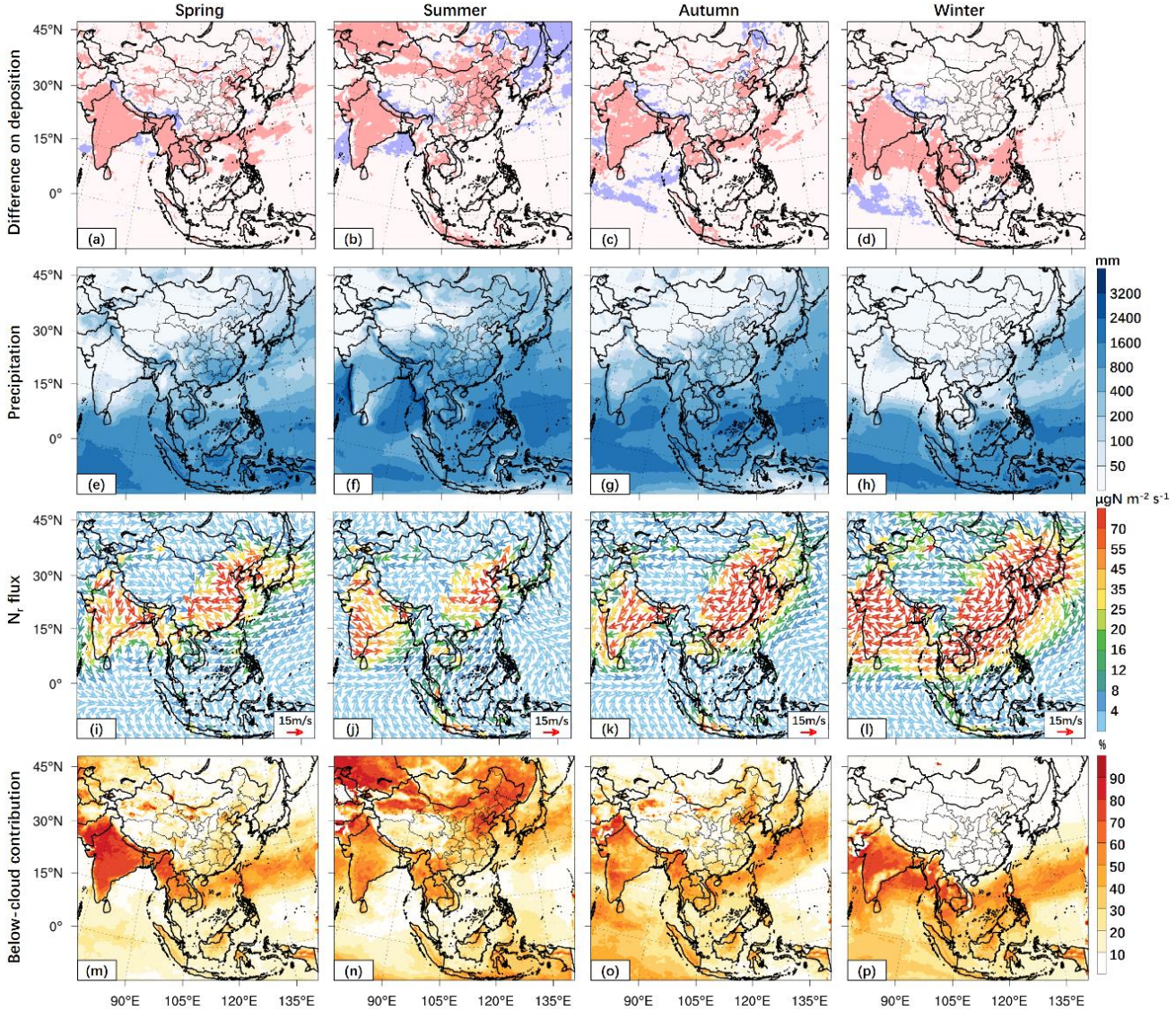

Figure 7. The first row (a-d) is the seasonal difference pattern between the Ge14-BWSC and Ge14-CAMx schemes on TIN wet deposition. The blue areas are the region where the TIN wet deposition of the Ge14-BWSC scheme is more than 5 % lower than that of the Ge14-CAMx scheme, while red areas where the TIN wet deposition of the Ge14-BWSC scheme is more than 5 % more than that of the Ge14-CAMx scheme. The second row (e-h) is the seasonal precipitation pattern. The third row (i-l) is the seasonal N_r species flux in the Ge14-BWSC scheme, and the fourth row (m-p) is the pattern of the TIN below-cloud contribution in the Ge14-BWSC scheme.

3.4 The influences on transport and wet deposition in downwind regions

The differences in the treatment of below-cloud wet scavenging of aerosols between the Ge14-BWSC and Ge14-CAMx schemes also cause the seasonal differences on their patterns of TIN wet deposition. In summer, the monsoon blows from Southeast Asia and the Northwest Pacific toward China, accompanied by the northward migration of the rain belt into China.

https://doi.org/10.5194/egusphere-2026-4057
Preprint. Discussion started: 20 August 2026

This increases the local TIN wet deposition through enhanced below-cloud scavenging in China, but decreases it in the Russian Far East and the Sea of Japan, which are downwind of Northeast China and Japan (The second column of Fig. 7). In winter, the monsoon blows from China toward Southeast Asia and the Northwest Pacific, accompanied by the southward migration of the rain belt into the equatorial region. the N_r species emitted from China are transported southward to the South China Sea and the Indochina Peninsula and undergo enhanced below-cloud wet scavenging and thereby increase local TIN wet deposition. As the N_r species are transported further south to the equatorial region, because a large amount of N_r species has already been scavenged, the wet deposition decreases there (The fourth column of Fig. 7). Some of the N_r species are transported to the East China Sea and Japan in winter, where they mainly undergo in-cloud scavenging; when transported further to the Northwest Pacific, the concentrations of N_r species are relatively low and can hardly cause a significant increase in wet deposition. In spring and autumn, the transition between summer and winter monsoons occurs, thereby the characteristics of differences on wet deposition at winter and summer are still present, but are not pronounced relative to winter and summer (The first and third column of Fig. 7). Notably, there is a belt of high below-cloud contribution of TIN within the domain, and it undergoes a seasonal migration along with the rain belt (The fourth row of Fig. 7). However, the seasonal characteristics of differences on the wet deposition between the Ge14-BWSC and Ge14 schemes are not noticeable. In all seasons, the main feature is decreased wet deposition over continental regions and the unchanged or slightly increased wet deposition over the equatorial sea area (Fig. S9).

4 Conclusions

This study proposed a new physically sound aerosol below-cloud scavenging scheme Ge14-BWSC, which effectively fixes the systematic biases of traditional wet deposition algorithms. The Ge14 scheme yields the highest annual wet deposition, followed by the Ge14-BWSC, Ge14-CAMx and CAMx schemes. This ranking agrees reasonably well with the simulated BWSC. However, the Ge14 scheme overestimates nitrogen concentration in precipitation by misapplying in-cloud scavenging coefficients and the CAMx/Ge14-CAMx schemes underestimate nitrogen levels due to weak below-cloud removal. The separation of in-cloud and below-cloud removal pathways and physically comprehensive and rational parameterization of below-cloud scavenging emphasized by the Ge14-BWSC scheme helps it improve the simulation of wet scavenging in polluted regions. This scheme achieves excellent consistency with field-observed below-cloud scavenging coefficients and fractions in Beijing and accurately reproduces the measured high TIN concentrations in precipitation exceeding 3.0 mgN L^{-1} over polluted regions including the BTH, YRD and Northeast China (NMB = -4 %). The inclusion of the new mechanisms increases the proportion of aerosols in below-cloud wet deposition, avoiding the situation that the below-cloud deposition relies almost solely on gaseous substances dominated by HNO_3 for N_{ox} and NH_3 for N_{rd} induced by traditional mechanisms. That is also the reason why some current CTMs (e.g. CAMx) artificially enlarge fine-mode aerosol sizes by a factor of 10 to strengthen below-cloud scavenging processes of aerosols. Besides, the updated mechanisms reasonably produce a greater enhancement of below-cloud contributions for N_{rd} compared with N_{ox}. This is consistent not

https://doi.org/10.5194/egusphere-2026-4057
Preprint. Discussion started: 20 August 2026

only with the contrasting emission heights, whereby NH_3 largely originates from near-surface sources, but also with the preferential formation of low-volatile $(NH_4)_2SO_4$ from particulate NH_4^+. This sulphate salt is efficiently removed by precipitation, in contrast to semi-volatile NH_4NO_3 subject to re-volatilization back to the atmosphere. Building on these results, the updated scavenging mechanisms reshape the spatial pattern of nitrogen wet deposition, where enhanced local removal within the seasonally shifting rain belt elevates inland polluted-area deposition yet suppresses downwind remote-region fluxes, and govern long-range transport of N_r under the control of seasonal migration of the rain belt and the transport of N_r from source regions. Although, the deposition and cross-regional transport is discussed in this paper, no quantitative source identification has yet been conducted for deposition within and below clouds. Further investigations will be carried out in the future. Overall, the improved scheme not only reduces biases in simulating nitrogen wet deposition in polluted regions, but also implies that current CTMs may systematically distort the export of nitrogen from source regions to remote oceans. These findings have broader implications for accurate modelling of nitrogen deposition, assessing nitrogen deposition-driven eutrophication, and the global nitrogen budget under changing precipitation patterns accompanied by climate change.

Code and data availability

The code and data are available upon request to the corresponding author by email.

Author contributions

This study was designed by BG and ZW. Model development was done by DX, NL and XC. Field data were collected and analyzed by DX and BG. Model simulation, validation and interpretation were done by NL, NY and QT. The manuscript was written by NL.

Competing interests

The authors declare that they have no conflicts of interest.

Acknowledgements

We acknowledge the CNEMC and EANET for providing observed wet deposition data over East Asia.

https://doi.org/10.5194/egusphere-2026-4057
Preprint. Discussion started: 20 August 2026

Financial support

This work was supported by the National Natural Science Foundation of China (Nos. 42122049 and 42377104), the National Key Scientific and Technological Infrastructure project "Earth System Science Numerical Simulator Facility" (EarthLab), and Natural Science Foundation of Chongqing, China (CSTB2024NSCQ-MSX1298).

References

Bae, S. Y., Jung, C. H., and Kim, Y. P.: Derivation and verification of an aerosol dynamics expression for the below-cloud scavenging process using the moment method, J. Aerosol. Sci., 41, 266-280, 10.1016/j.jaerosci.2009.11.006, 2010.

Cerro, C., Codina, B., Bech, J., and Lorente, J.: Modeling raindrop size distribution and Z(R) relations in the Western Mediterranean area, J. Appl. Meteorol., 36, 1470-1479, 10.1175/1520-0450(1997)036<1470:Mrsdaz>2.0.Co;2, 1997.

Chatterjee, A., Jayaraman, A., Rao, T. N., and Raha, S.: In-cloud and below-cloud scavenging of aerosol ionic species over a tropical rural atmosphere in India, J. Atmos. Chem., 66, 27-40, 10.1007/s10874-011-9190-5, 2010.

Chen, H. S.: Development of Global Multi-scale Nested Atmospheric Chemical Transport Model (GNAQPMS) and Its Application to Atmospheric Mercury Transport (in Chinese), Doctor, Atmospheric Physics and Atmospheric Environment, Institute of Atmospheric Physics, Chinese Academy of Sciences, Beijing, 162 pp., 2013.

de Wolf, D. A.: On the Laws-Parsons distribution of raindrop sizes, Radio Sci., 36, 639-642, 10.1029/2000rs002369, 2001.

Du, E.: A database of annual atmospheric acid and nutrient deposition to China's forests, Sci. Data, 5, 180223-180223, 10.1038/sdata.2018.223, 2018.

ENVIRON.INC: User's Guide Comprehensive Air Quality Model with Extensions (CAMx) Version 6, 773 San Marin Drive, Suite 2115, Novato, California, 310 pp.2013.

Fang, S., Zhuang, S. H., Goto, D., Hu, X. F., Li, S., and Huang, S. X.: Coupled modeling of in- and below-cloud wet deposition for atmospheric 137Cs transport following the Fukushima Daiichi accident using WRF-Chem: A self-consistent evaluation of 25 scheme combinations, Environ. Int., 158, 16, 10.1016/j.envint.2021.106882, 2022.

Feingold, G. and Levin, Z.: The lognormal fit to raindrop spectra from frontal convective clouds in israel, Journal of Climate and Applied Meteorology, 25, 1346-1363, 10.1175/1520-0450(1986)025<1346:Tlftrs>2.0.Co;2, 1986.

Ge, B. Z., Wang, Z. F., Gbaguidi, A. E., and Zhang, Q. X.: Source Identification of Acid Rain Arising over Northeast China: Observed Evidence and Model Simulation, Aerosol Air Qual. Res., 16, 1366-1377, 10.4209/aaqr.2015.05.0294, 2016.

Ge, B. Z., Wang, Z. F., Xu, X. B., Wu, J. B., Yu, X. L., and Li, J.: Wet deposition of acidifying substances in different regions of China and the rest of East Asia: Modeling with updated NAQPMS, Environ. Pollut., 187, 10-21, 10.1016/j.envpol.2013.12.014, 2014.

Ge, B. Z., Xu, D. H., Wild, O., Yao, X. F., Wang, J. H., Chen, X. S., Tan, Q. X., Pan, X. L., and Wang, Z. F.: Inter-annual variations of wet deposition in Beijing from 2014-2017: implications of below-cloud scavenging of inorganic aerosols, Atmos. Chem. Phys., 21, 9441-9454, 10.5194/acp-21-9441-2021, 2021.

https://doi.org/10.5194/egusphere-2026-4057
Preprint. Discussion started: 20 August 2026

Ge, B. Z., Itahashi, S., Sato, K., Xu, D. H., Wang, J. H., Fan, F., Tan, Q. X., Fu, J. S., Wang, X. M., Yamaji, K., Nagashima, T., Li, J., Kajino, M., Liao, H., Zhang, M. G., Wang, Z., Li, M., Woo, J. H., Kurokawa, J., Pan, Y. P., Wu, Q. Z., Liu, X. J., and Wang, Z. F.: Model Inter-Comparison Study for Asia (MICS-Asia) phase III: multimodel comparison of reactive nitrogen deposition over China, Atmos. Chem. Phys., 20, 10587-10610, 10.5194/acp-20-10587-2020, 2020.

Guenther, A., Karl, T., Harley, P., Wiedinmyer, C., Palmer, P. I., and Geron, C.: Estimates of global terrestrial isoprene emissions using MEGAN (Model of Emissions of Gases and Aerosols from Nature), Atmos. Chem. Phys., 6, 3181-3210, 10.5194/acp-6-3181-2006, 2006.

Guo, Y. H.: Study on the characteristics of atmospheric environmental quality of oasis cities in arid region of Xinjiang and numerical simulation (in Chinese), Doctor, Atmospheric Physics and Atmospheric Environment, Institute of Atmospheric Physics, Chinese Academy of Sciences, Beijing, 221 pp., 2013.

Itahashi, S., Yamaji, K., Chatani, S., Hisatsune, K., Saito, S., and Hayami, H.: Model Performance Differences in Sulfate Aerosol in Winter over Japan Based on Regional Chemical Transport Models of CMAQ and CAMx, Atmosphere, 9, 17, 10.3390/atmos9120488, 2018.

Itahashi, S., Ge, B. Z., Sato, K., Fu, J. S., Wang, X. M., Yamaji, K., Nagashima, T., Li, J., Kajino, M., Liao, H., Zhang, M. G., Wang, Z., Li, M., Kurokawa, J., Carmichae, G. R., and Wang, Z. F.: MICS-Asia III: overview of model intercomparison and evaluation of acid deposition over Asia, Atmos. Chem. Phys., 20, 2667-2693, 10.5194/acp-20-2667-2020, 2020.

Kulshrestha, U. C., Reddy, L. A. K., Satyanarayana, J., and Kulshrestha, M. J.: Real-time wet scavenging of major chemical constituents of aerosols and role of rain intensity in Indian region, Atmos. Environ., 43, 5123-5127, 10.1016/j.atmosenv.2009.07.025, 2009.

Laakso, L., Grönholm, T., Rannik, Ü., Kosmale, M., Fiedler, V., Vehkamäki, H., and Kulmala, M.: Ultrafine particle scavenging coefficients calculated from 6 years field measurements, Atmos. Environ., 37, 3605-3613, 10.1016/s1352-2310(03)00326-1, 2003.

Li, J., Wang, Z. F., Zhuang, G., Luo, G., Sun, Y., and Wang, Q.: Mixing of Asian mineral dust with anthropogenic pollutants over East Asia: a model case study of a super-duststorm in March 2010, Atmos. Chem. Phys., 12, 7591-7607, 10.5194/acp-12-7591-2012, 2012.

Li, J., Wang, Z., Akimoto, H., Yamaji, K., Takigawa, M., Pochanart, P., Liu, Y., Tanimoto, H., and Kanaya, Y.: Near-ground ozone source attributions and outflow in central eastern China during MTX2006, Atmos. Chem. Phys., 8, 7335-7351, 10.5194/acp-8-7335-2008, 2008.

Li, J., Wang, Z., Wang, X., Yamaji, K., Takigawa, M., Kanaya, Y., Pochanart, P., Liu, Y., Irie, H., Hu, B., Tanimoto, H., and Akimoto, H.: Impacts of aerosols on summertime tropospheric photolysis frequencies and photochemistry over Central Eastern China, Atmos. Environ., 45, 1817-1829, 10.1016/j.atmosenv.2011.01.016, 2011.

Li, M., Kurokawa, J., Zhang, Q., Woo, J. H., Morikawa, T., Chatani, S., Lu, Z. F., Song, Y., Geng, G. N., Hu, H. W., Kim, J., Cooper, O. R., and McDonald, B. C.: MIXv2: a long-term mosaic emission inventory for Asia (2010-2017), Atmos. Chem. Phys., 24, 3925-3952, 10.5194/acp-24-3925-2024, 2024.

https://doi.org/10.5194/egusphere-2026-4057
Preprint. Discussion started: 20 August 2026

Li, M., Zhang, Q., Kurokawa, J., Woo, J. H., He, K. B., Lu, Z. F., Ohara, T., Song, Y., Streets, D. G., Carmichael, G. R., Cheng, Y. F., Hong, C. P., Huo, H., Jiang, X. J., Kang, S. C., Liu, F., Su, H., and Zheng, B.: MIX: a mosaic Asian anthropogenic emission inventory under the international collaboration framework of the MICS-Asia and HTAP, Atmos. Chem. Phys., 17, 935-963, 10.5194/acp-17-935-2017, 2017.

Lu, X. C. and Fung, J. C. H.: Sensitivity assessment of $PM_{2.5}$ simulation to the below-cloud washout schemes in an atmospheric chemical transport model, Tellus Ser. B-Chem. Phys. Meteorol., 70, 1-17, 10.1080/16000889.2018.1476435, 2018.

Lue, C. Q. and Tian, H. Q.: Spatial and temporal patterns of nitrogen deposition in China: Synthesis of observational data, J. Geophys. Res.-Atmos., 112, 10.1029/2006jd007990, 2007.

Luo, G., Yu, F. Q., and Schwab, J.: Revised treatment of wet scavenging processes dramatically improves GEOS-Chem 12.0.0 simulations of surface nitric acid, nitrate, and ammonium over the United States, Geoscientific Model Development, 12, 3439-3447, 10.5194/gmd-12-3439-2019, 2019.

Mircea, M. and Stefan, S.: A theoretical study of the microphysical parameterization of the scavenging coefficient as a function of precipitation type and rate, Atmos. Environ., 32, 2931-2938, 10.1016/s1352-2310(98)00018-1, 1998.

Pan, Y. P., Zhu, X. Y., Tian, S. L., Wang, L. L., Zhang, G. Z., Zhou, Y. B., Xu, P., Hu, B., and Wang, Y. S.: Wet deposition and scavenging ratio of air pollutants during an extreme rainstorm in the North China Plain, Atmospheric and Oceanic Science Letters, 10, 348-353, 10.1080/16742834.2017.1343084, 2017.

Ponette-Gonzalez, A. G., Lewis, H., Henderson, B. H., Carnelos, D., Pineiro, G., Weathers, K. C., and Schwede, D. B.: Wet nitrogen (N) deposition to urban Latin America: Filling in the gaps with GEOS-Chem, Atmos. Environ., 278, 8, 10.1016/j.atmosenv.2022.119095, 2022.

Ramboll.INC: User's Guide Comprehensive Air Quality Model with Extensions (CAMx) Version 7.3, 383 pp.2024.

Rastogi, N. and Sarin, M. M.: Chemical characteristics of individual rain events from a semi-arid region in India: Three-year study, Atmos. Environ., 39, 3313-3323, 10.1016/j.atmosenv.2005.01.053, 2005.

Roselle, S. J. and Binkowski, F. S.: Science algorithms of the EPA Models-3 Community multiscale air quality modeling system, Chapter 11: Cloud dynamics and chemistry, 1999.

Ryu, Y. H. and Min, S. K.: Improving Wet and Dry Deposition of Aerosols in WRF-Chem: Updates to Below-Cloud Scavenging and Coarse-Particle Dry Deposition, J. Adv. Model. Earth Syst., 14, 16, 10.1029/2021ms002792, 2022.

Seinfeld, J. H. and Pandis, S. N.: Atmospheric chemistry and physics: from air pollution to climate change, John Wiley & Sons2006.

Shimadera, H., Kojima, T., Kondo, A., and Inoue, Y.: Performance comparison of CMAQ and CAMx for one-year $PM_{2.5}$ simulation in Japan, Int. J. Environ. Pollut., 57, 146-161, 10.1504/ijep.2015.074498, 2015.

Simpson, D., Fagerli, H., Jonson, J. E., Tsyro, S., Wind, P., and Tuovinen, J.-P.: Wet deposition. Transboundary acidification, eutrophication and ground level ozone in Europe. EMEP Report 1/2003, Norwegian Meteorological Institute, Oslo, Norway.2003.

https://doi.org/10.5194/egusphere-2026-4057
Preprint. Discussion started: 20 August 2026

Skamarock, W. C., Klemp, J., Dudhia, J., Gill, D., Liu, Z., Berner, J., Wang, W., Powers, J., Duda, M., and Barker, D.: A description of the advanced research WRF model version 4 (Vol. 145), J National Center for Atmospheric Research, 2019.

Tan, J. N., Su, H., Itahashi, S., Tao, W., Wang, S. W., Li, R., Fu, H. B., Huang, K., Fu, J. S., and Cheng, Y. F.: Quantifying the wet deposition of reactive nitrogen over China: Synthesis of observations and models, Science of the Total Environment, 851, 10.1016/j.scitotenv.2022.158007, 2022.

Tang, X. Y., Zhang, Y. H., and Shao, M.: Atmospheric Environmental Chemistry Version 2 (in Chinese), Beijing2006.

Theobald, M. R., Vivanco, M. G., Aas, W., Andersson, C., Ciarelli, G., Couvidat, F., Cuvelier, K., Manders, A., Mircea, M., Pay, M. T., Tsyro, S., Adani, M., Bergström, R., Bessagnet, B., Briganti, G., Cappelletti, A., D'Isidoro, M., Fagerli, H., Mar, K., Otero, N., Raffort, V., Roustan, Y., Schaap, M., Wind, P., and Colette, A.: An evaluation of European nitrogen and sulfur wet deposition and their trends estimated by six chemistry transport models for the period 1990-2010, Atmos. Chem. Phys., 19, 379-405, 10.5194/acp-19-379-2019, 2019.

van der Werf, G. R., Randerson, J. T., Giglio, L., Collatz, G. J., Mu, M., Kasibhatla, P. S., Morton, D. C., DeFries, R. S., Jin, Y., and van Leeuwen, T. T.: Global fire emissions and the contribution of deforestation, savanna, forest, agricultural, and peat fires (1997-2009), Atmos. Chem. Phys., 10, 11707-11735, 10.5194/acp-10-11707-2010, 2010.

Vet, R., Artz, R. S., and Carou, S.: Preface to: A global assessment of precipitation chemistry and deposition of sulfur, nitrogen, sea salt, base cations, organic acids, acidity and pH, and phosphorus Preface, Atmos. Environ., 93, 1-2, 10.1016/j.atmosenv.2013.11.013, 2014.

Wang, X., Zhang, L., and Moran, M. D.: Uncertainty assessment of current size-resolved parameterizations for below-cloud particle scavenging by rain, Atmos. Chem. Phys., 10, 5685-5705, 10.5194/acp-10-5685-2010, 2010.

Wang, X., Zhang, L., and Moran, M. D.: Development of a new semi-empirical parameterization for below-cloud scavenging of size-resolved aerosol particles by both rain and snow, Geoscientific Model Development, 7, 799-819, 10.5194/gmd-7-799-2014, 2014a.

Wang, Y., Zhu, B., Kang, H. Q., Gao, J. H., Jiang, Q., and Liu, X. H.: Theoretical and observational study on below-cloud rain scavenging of aerosol particles, Journal of University of Chinese Academy of Sciences, 31, 306-313, 2014b.

Wang, Z. F., Li, J., Wang, X. Q., Pochanart, P., and Akimoto, H.: Modeling of regional high ozone episode observed at two mountain sites (Mt. Tai and Huang) in East China, J. Atmos. Chem., 55, 253-272, 10.1007/s10874-006-9038-6, 2006.

Wang, Z. F., Xie, F. Y., Sakurai, T., Ueda, H., Han, Z. W., Carmichael, G. R., Streets, D., Engardt, M., Holloway, T., Hayami, H., Kajino, M., Thongboonchoo, N., Bennet, C., Park, S. U., Fung, C., Chang, A., Sartelet, K., and Amann, M.: MICS-Asia II: Model inter-comparison and evaluation of acid deposition, Atmos. Environ., 42, 3528-3542, 10.1016/j.atmosenv.2007.12.071, 2008.

Wang, Z. F., Li, X. W., Gao, M., Ge, B. Z., Tang, X., Chen, X. S., Wu, Q. Z., Wu, L., Wang, Z., Yang, T., Pan, X. L., Chen, H. S., Wu, H. J., Li, J. X., Wang, W. D., Kong, L., Du, H. Y., Cao, K., Zhu, M. M., Wang, Z. X., Wang, T., Wang, F., Wu, Z. C., and Li, J.: Advances and Perspectives in Atmospheric Environment Modeling in China, Adv. Atmos. Sci., 25, 10.1007/s00376-026-5677-5, 2026.

https://doi.org/10.5194/egusphere-2026-4057
Preprint. Discussion started: 20 August 2026

Xu, D. H., Ge, B. Z., Chen, X. S., Sun, Y. L., Cheng, N. L., Li, M., Pan, X. L., Ma, Z. Q., Pan, Y. P., and Wang, Z. F.: Multi-method determination of the below-cloud wet scavenging coefficients of aerosols in Beijing, China, Atmos. Chem. Phys., 19, 15569-15581, 10.5194/acp-19-15569-2019, 2019a.

Xu, D. H., Ge, B. Z., Wang, Z. F., Sun, Y. L., Chen, Y., Ji, D. S., Yang, T., Ma, Z. Q., Cheng, N. L., Hao, J. Q., and Yao, X. F.: Below-cloud wet scavenging of soluble inorganic ions by rain in Beijing during the summer of 2014, Environ. Pollut., 230, 963-973, 10.1016/j.envpol.2017.07.033, 2017.

Xu, W., Zhang, L., and Liu, X. J.: A database of atmospheric nitrogen concentration and deposition from the nationwide monitoring network in China, Sci. Data, 6, 6, 10.1038/s41597-019-0061-2, 2019b.

Xu, W., Liu, L., Cheng, M. M., Zhao, Y. H., Zhang, L., Pan, Y. P., Zhang, X. M., Gu, B. J., Li, Y., Zhang, X. Y., Shen, J. L., Lu, L., Luo, X. S., Zhao, Y., Feng, Z. Z., Collett, J. L., Zhang, F. S., and Liu, X. J.: Spatial-temporal patterns of inorganic nitrogen air concentrations and deposition in eastern China, Atmos. Chem. Phys., 18, 10931-10954, 10.5194/acp-18-10931-2018, 2018.

Xu, W., Luo, X. S., Pan, Y. P., Zhang, L., Tang, A. H., Shen, J. L., Zhang, Y., Li, K. H., Wu, Q. H., Yang, D. W., Zhang, Y. Y., Xue, J., Li, W. Q., Li, Q. Q., Tang, L., Lu, S. H., Liang, T., Tong, Y. A., Liu, P., Zhang, Q., Xiong, Z. Q., Shi, X. J., Wu, L. H., Shi, W. Q., Tian, K., Zhong, X. H., Shi, K., Tang, Q. Y., Zhang, L. J., Huang, J. L., He, C. E., Kuang, F. H., Zhu, B., Liu, H., Jin, X., Xin, Y. J., Shi, X. K., Du, E. Z., Dore, A. J., Tang, S., Collett, J. L., Goulding, K., Sun, Y. X., Ren, J., Zhang, F. S., and Liu, X. J.: Quantifying atmospheric nitrogen deposition through a nationwide monitoring network across China, Atmos. Chem. Phys., 15, 12345-12360, 10.5194/acp-15-12345-2015, 2015.

Yao, L. Q., Kong, S. F., Nemitz, E., Vieno, M., Cheng, Y., Zheng, H., Wang, Y. L., Chen, N., Hu, Y., Liu, D. T., Zhao, T. L., Bai, Y. Q., and Qi, S. H.: Improving Below-Cloud Scavenging Coefficients of Sulfate, Nitrate, and Ammonium in $PM_{2.5}$ and Implications for Numerical Simulation and Air Pollution Control, J. Geophys. Res.-Atmos., 129, 23, 10.1029/2023jd039487, 2024.

Yu, G. R., Jia, Y. L., He, N. P., Zhu, J. X., Chen, Z., Wang, Q. F., Piao, S. L., Liu, X. J., He, H. L., Guo, X. B., Wen, Z., Li, P., Ding, G. A., and Goulding, K.: Stabilization of atmospheric nitrogen deposition in China over the past decade, Nature Geoscience, 12, 424-+, 10.1038/s41561-019-0352-4, 2019.

Zhang, Y., Ge, B. Z., Chen, G. H., Wang, D., Li, F. L., Fu, J. S., Liu, X. J., and Wang, Z. F.: Consecutive wet deposition of nitrogen along half of China's coastal cities induced by Super Typhoon Muifa (2022) with multiple landfalls, Journal of Environmental Sciences, 156, 126-138, 10.1016/j.jes.2024.11.004, 2025.

Zhang, Y., Su, X. T., Ge, B. Z., Xu, X. B., Tan, Q. X., Chen, G. H., Xu, D. H., Chen, X. S., Wu, L., Gao, M., Pan, X. L., Guo, J. P., Liu, X. J., Fu, J. S., and Wang, Z. F.: Enhanced Wet Deposition of Nitrogen Induced by a Landfalling Typhoon over East Asia: Implications for the Marine Eco-Environment, Environmental Science & Technology Letters, 9, 1014-1021, 10.1021/acs.estlett.2c00762, 2022.

Zhao, S. P., Yu, Y., He, J. J., Yin, D. Y., and Wang, B.: Below-cloud scavenging of aerosol particles by precipitation in a typical valley city, northwestern China, Atmos. Environ., 102, 70-78, 10.1016/j.atmosenv.2014.11.051, 2015.